Journal of Applied Polymer Science

Effect of block composition on the morphology, hydration, and transport properties of sulfonated PS-*b*-PEGPEM-*b*-PS

Maritza Pérez-Pérez, David Suleiman
Chemical Engineering Department, University of Puerto Rico, Mayagüez Puerto Rico 00681-9000
Correspondence to: D. Suleiman (E-mail: david.suleiman@upr.edu)

ABSTRACT: This work discusses the effect of block composition on the properties of proton conducting polymer membranes. A homopolymer and two block copolymers were synthesized using atom transfer radical polymerization. The homopolymer poly(ethylene glycol phenyl ether methacrylate) (PEGPEM) was used as a bifunctional macroinitiator. Polystyrene (PS), was added to both sides of PEGPEM (A) with two different percentages of PS (B) (i.e., 18 and 31%). These copolymers, BAB 18, BAB 31 and the homopolymer A, were completely sulfonated (SA, SBAB 18 and SBAB 31). The resulting polymers produced different water absorption values and transport properties for direct methanol fuel cell (DMFC) applications. The nanostructure and morphology of the casted membranes were studied using small-angle X-ray scattering and atomic force microscopy. The results revealed that all six membranes exhibited a disordered phase-segregated morphology, which changed on sulfonation into small-interconnected ionic domains. Normalized DMFC selectivities (proton conductivity over methanol permeability divided by the respective values for Nafion®) were calculated and ranged from 1.16 (SBAB 31) to 15.30 (BAB 18), indicating that the performance of these materials can be comparable or better than Nafion®. Transport property results also suggest that chemistry (block nature and composition), morphology and water content play a critical role in the transport mechanism of protons and methanol. For example, the percentage of B in BAB 18 provides shorter interstitial ionic distances and sufficient water content to produce high proton conductivity, while maintaining low methanol permeability in a multi-ionic proton exchange membrane. © 2016 Wiley Periodicals, Inc. J. Appl. Polym. Sci. **2016**, *133*, 44343.

KEYWORDS: conducting polymers; copolymers; membranes; morphology

Received 2 May 2016; accepted 2 August 2016
DOI: 10.1002/app.44343

INTRODUCTION

Fuel cells are a promising power source for clean energy and portable applications.[1–4] There are several types of fuel cells such as, proton exchange membrane fuel cell (PEMFC), and direct methanol fuel cell (DMFC).[4] PEMFC uses hydrogen as the fuel while DMFC uses methanol. The performance of PEMFC is higher than DMFC; however, DMFC possesses several advantages; such that it could be used at ambient temperatures, in addition to overcoming the storage, handling, and safety issues associated with hydrogen.[5]

In a fuel cell, one of the main components is the proton exchange membrane (PEM).[4,6–10] A PEM is a proton conducting polymer membrane that allows the transport of protons while blocking the passage of fuel through the membrane.[9] PEM's must also possess high thermomechanical and chemical stability to the fuel conditions.[8] The most promising fuel cell devices are the PEMFC and the DMFC.[4]

The ability to conduct protons through the membrane has been related to the acid and water content of the membrane and the chemical structure and morphology of the membrane.[8] "Proton hopping" or "Grotthus mechanism" has been used to describe the transport mechanism of protons through the ionic domains in the PEM.[9] This diffusion mechanism is used to describe the transport of protons through the PEM assisted by the water molecules near the ionic domains.[9,11] Proton transport is also affected by the effective mean-free path of connectivity of the conduction pathways in the membrane.[8] The distance between acid groups also affects the proton mobility. Larger distances between the acid groups are expected to require greater energy in comparison to shorter distances, leading to lower proton mobility, and therefore, lower proton conductivity.[12,13]

The state-of-the-art PEM is the perfluorosulfonic membrane Nafion®.[3,8,11–20] The presence of polar and nonpolar moieties in Nafion® produces phase segregation, which is desirable for DMFC transport properties.[8] However, this microstructure also allows methanol crossover which limits its performance for DMFC applications.[4] Because of its high methanol permeability, several efforts have been made to modify Nafion® or develop alternative polymers for DMFC applications. Several researchers have developed new polymers of lower cost, while maintaining

high proton conductivity and low methanol permeability.[21,22] Many promising polymers are based on sulfonated aromatic segments such as PEEK.[20]

The synthesis of polymers with multi-ionic domains is proposed in this investigation to promote phase segregation in the membrane and to evaluate the role of the different ionic and non-ionic domains in the transport of protons and methanol through the PEM. This article presents the synthesis of poly(-ethylene glycol phenyl ether methacrylate) (PEGPEM) and poly(styrene)-*b*-poly(ethylene glycol phenyl ether methacrylate)-*b*-poly(styrene) (PS-*b*-PEGPEM-*b*-PS) with 18 and 31% of PS. The homopolymer and the block copolymers were sulfonated to increase the amount of ionic domains and to create synergism with the ether and ester domains. Transport properties for DMFC applications were evaluated and the results were explained with a chemical and morphological characterization using techniques such as Fourier transform infrared, small-angle X-ray scattering (SAXS), and atomic force microscopy (AFM).

EXPERIMENTAL

Materials

Chemicals used include: sulfuric acid (Sigma Aldrich, 95–98%), acetic anhydride (Aldrich Chemical, 99+%), methanol (Fisher Scientific, 99.9%), toluene (Fisher, 99.9%), and methylene chloride (Fisher, 99.9%). Other chemicals used include: 2, 2′-dipyridyl Bipy (Acros Organics, extra pure, 99%), copper (I) chloride (Acros-Organics, 99%), and ∝, ∝-dichlorotoluene (Aldrich, 95%) were used as received. Monomers used include ethylene glycol phenyl ether methacrylate (Sigma Aldrich, 99%, inhibited with 200 ppm monomethyl ether hydroquinone) and styrene (Acros-Organics, 99% inhibited with 4-*tert-butyl* catechol). All monomers were passed through an inhibitor remover (disposable column from Sigma-Aldrich).

Polymer Synthesis

The homopolymer, ethylene glycol phenyl ether methacrylate (EGPEM), was synthesized by atom transfer radical polymerization (ATRP) as follow: a mixture of 30 mL toluene, 30 mL EGPEM, 0.155 g copper chloride (CuCl), 0.491 g 2,2′-dipyridyl (bipy), and 0.03 mL of ∝,∝ dichlorotoluene was added to a 100 mL Schlenk reactor equipped with a magnetic stir bar. Figure 1 shows the synthesis of the homopolymer and the block copolymer. Afterwards, the Schlenk reactor was degassed with three cycles of thawing under a nitrogen atmosphere. The reactor was heated until it reached 110 °C and was left at this temperature for 24 h. Subsequently, the reaction was diluted by adding more toluene, filtered to remove the catalyst, and the polymer was precipitated on the addition of methanol. The final homopolymer possessed a yield of 87% and a molecular weight of 11,839 g/mol.

PEGPEM was used as macro initiator for the synthesis of the block copolymers with polystyrene (PS). 8.732 g of PEGPEM were dissolved in 30 mL of toluene in a 100 mL Schlenk reactor. 5 mL of styrene, 0.043 g CuCl, and 0.136 g bipy were added to the Schlenk reactor once the polymer was completely dissolved. The Schlenk reactor was degassed three times and left under a nitrogen atmosphere. The reactor was heated until a temperature of 110 °C was reached and left at that temperature for 24 h. Afterwards, the reaction was diluted by adding more toluene and filtered to remove the catalyst. The polymer was precipitated by the addition of methanol. The final block copolymer possessed a yield of 87% and a molecular weight of 22,295 g/mol. The same procedure was used for the polymer with 18% of PS (Mn = 14,564 g/mol).

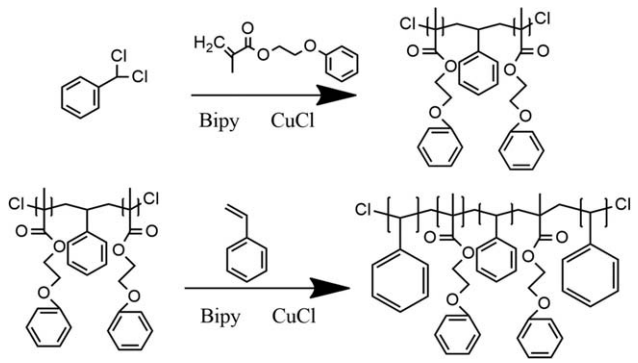

Figure 1. ATRP reaction used for the synthesis of the homopolymer and block copolymers.

Nomenclature

Table I summarizes the nomenclature used. A is for PEGPEM, B for PS, and S stands for sulfonated.

Polymer Sulfonation

The sulfonation of the polymers was performed using the suggested procedure described by Elabd and Napadensky.[23] Figure 2 shows the sulfonation reactions and the chemical structure of the sulfonated polymers. 10 g of the polymer were dried for 24 h at 60 °C and dissolved in methylene chloride (5% wt/v). The sulfonating agent (i.e., acetyl sulfate) was prepared by cooling 130 mL of methylene chloride in an ice bath for 10 min. The ratio of acetyl sulfate to polymer was 1:1 (one sulfonic group per aromatic ring). 6 mL of acetic anhydride were then added to the cooled methylene chloride under constant stirring. After 10 min, 3 mL of sulfuric acid was added to the acetic anhydride. Finally, after 10 min the sulfonating agent was slowly added to the polymer solution to begin the sulfonation reaction. The reaction was terminated after 10 min, when the polymer precipitated at the bottom of the reactor. Then, the solvents were allowed to evaporate at room temperature for 4 days. The reacted polymer was washed several times with cold DI water until the pH of the water became neutral. The polymer was then dried at 60 °C for 48 h.

Table I. Polymer Nomenclature

Abbreviated polymer name	Letter
PEGPEM	A
PS-*b*-PEGPEM-*b*-PS 18%	BAB 18
PS-*b*-PEGPEM-*b*-PS 31%	BAB 31
Sulfonated PEGPEM	SA
Sulfonated PS-*b*-PEGPEM-*b*-PS 18%	SBAB 18
Sulfonated PS-*b*-PEGPEM-*b*-PS 31%	SBAB 31

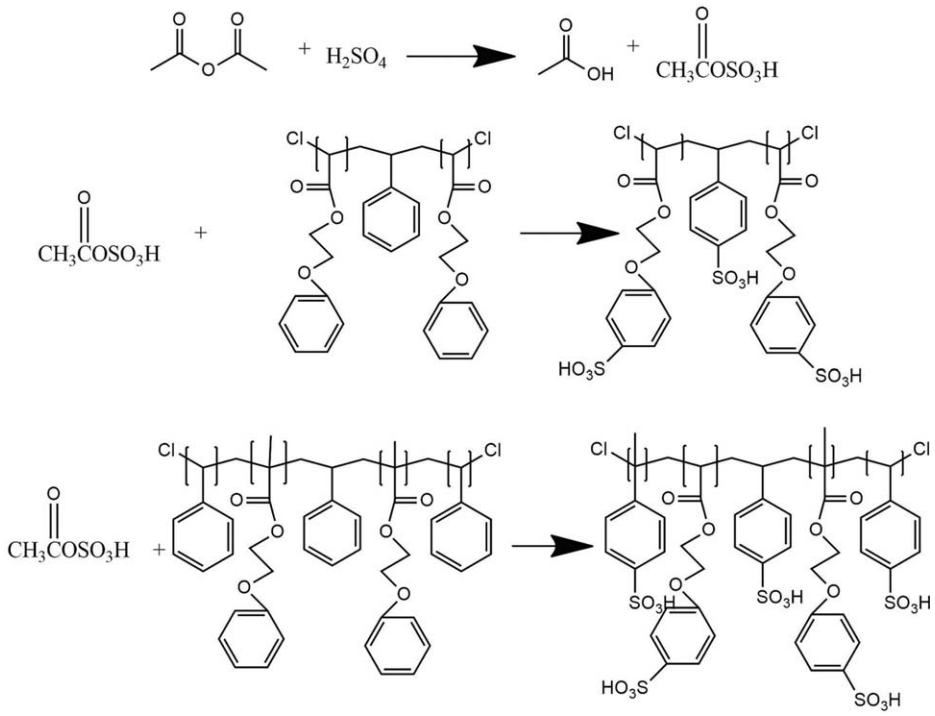

Figure 2. Sulfonation reaction of the homopolymer and block copolymers.

Membrane Casting

Membranes were prepared using the method of solvent casting. PEGPEM was dissolved in toluene with a polymer concentration of 5 wt %. The solution was casted in a Teflon® Petri dish for 2 days at 60 °C to allow the evaporation of the solvent. PS-*b*-PEGPEM-*b*-PS membranes were prepared using the same procedure as PEGPEM while sulfonated membranes were casted using hot water as the solvent.

Polymer Characterization

Gel Permeation Analysis. Gel Permeation Chromatography was conducted to obtain the molecular weight of the homopolymer and the block copolymers. The measurements were performed by the Soft Materials' Laboratory of the College of Engineering at the University of Wisconsin-Madison. The samples were dissolved in THF at a concentration of 0.25% (weight/volume) and ran through a set of two PolyPore 5μm mixed gel columns (Agilent Technology) at a flow rate 1 mL/min at 40 °C. The columns were calibrated with PS standards (PS-2) with a molecular weight range from 400k Daltons to 500 Daltons (Varian, Inc.) The samples were analyzed against a standard curve of PS.

Elemental Analysis. Elemental Analysis (EA) was performed by Atlantic Microlab (Norcross, GA) to obtain the weight fraction of C, H, S, and O, which were used to determine the sulfonation level using stoichiometric calculations.

Fourier Transform Infrared. Fourier transform infrared (FT-IR) spectroscopy was used to confirm the presence of the different functional groups and to determine if there were any shifts in the characteristic bands on sulfonation and hydration. The infrared spectra of the different samples were collected using an ALPHA Platinum Bruker with a Diamond ATR holder within a wave number range of 600 to 1800 cm^{-1} using 200 scans at a 2 cm^{-1} resolution.

Ion Exchange Capacity. Ion exchange capacity (IEC) measured the ability of the ionic polymer membranes to undergo displacement of ions previously attached (protons in sulfonic domains) or loosely incorporated into its structure (protons in hydrated ester or ether domains). The IEC was measured immersing the pre-dried (i.e., dried at 60 °C for 24 h) membrane in a 1.0 *M* solution of NaCl for 24 h. The membrane was then removed from the solution. The solution was titrated using a 0.01 *M* solution of NaOH until the pH was neutral. The IEC was calculated using the moles of ions per mass of dried polymer membrane as described in eq. (1).

$$\mathrm{IEC}\left(\frac{\text{mequiv.}}{\text{g}}\right)=\frac{V_{\mathrm{NaOH}}\times C_{\mathrm{NaOH}}}{W_{\mathrm{dry}}} \tag{1}$$

where V_{NaOH} is the volume of NaOH required for titration, C_{NaOH} is the molar concentration of NaOH, and W_{dry} is the weight of the dried membrane. As Na^+ was the ion exchanged in all membranes, and other investigations with sulfonated polymers measured one Na^+ for each sulfonic domain,[24] the mequiv. (mmoles) of ionic domain represented either the ether or ester domains for the unsulfonated polymers, or the sulfonic, ester, and ether domains for the sulfonated polymer membranes.

Water Uptake. Water uptake measurements started with a membrane dried at 60 °C for 24 h; its weight was recorded before starting the exposure of the membrane to water. The samples were immersed in an excess of DI water at 25 °C. The weight of the wet membrane was measured after removing the excess water from its surface. This was achieved by blotting it

with a tissue paper at different times until the weight of the membrane was constant. Water uptake was calculated using eq. (2).

$$\text{Water uptake} = \frac{W_{wet} - W_{dry}}{W_{dry}} \times 100 \quad (2)$$

where W_{wet} and W_{dry} are the wet and dry weight of the membrane, respectively.

Water Content. The average number of water molecules per ionic domain (water content), also called λ was calculated using the experimental values of water uptake (mass water/mass dry polymer) and IEC (mequiv./mass dry polymer) [eq. (3)].

$$\frac{[H_2O]}{[\text{ionic domain}]} = \lambda = \frac{\text{water uptake (\%)} \times 10}{18 \times \text{IEC}\left(\frac{\text{mmol}}{\text{g}}\right)} \quad (3)$$

Although λ describes the moles of water per mole of ionic domain, it cannot distinguish between the water close to an ether, ester or sulfonic domain, because the original measurements (water uptake and IEC) cannot differentiate the water coordination.

Morphology Characterization

Small-Angle X-ray Scattering. SAXS measurements for dry and hydrated membranes of A and BAB were performed using an Anton Paar SAXSpace. Two-dimensional scattering patterns were collected on a pinhole-collimated system using image plates and read by a Cyclone® Plus PerkinElmer image plate reader. The SAXS Quant software® was used to reduce two-dimensional data to one-dimensional intensity versus scattering vector (q) plots. The X-ray wavelength used was 1.54 Å. The scattering vector, q, was related to the interstitial distance between atoms using Bragg's Law [eq. (4)]

$$d_{Bragg} = \frac{2\pi}{q_{Bragg}} \quad (4)$$

where d_{Bragg} is the interstitial distance between atoms and q_{Bragg} is the scattering vector.

Atomic Force Microscopy. AFM was performed using an Agilent AFM 550 in AC imaging mode. All measurements were performed at room temperature. The phase images were recorded with a resolution of 256 and a scanning speed of 2.01 lines/s.

Transport Properties

Proton Conductivity. The proton conductivity (σ) of the membranes was measured using a Fuel Cell Test System (850e Multi Range) equipped with a 885 Fuel Cell Potentiostat from Scribner Associate Inc., over a frequency range of 0.1 Hz to 1.0 MHz. The membranes were first immersed in an excess of DI water. The temperature was set at 60 °C and the air used in the cathode and hydrogen in the anode contained 100% relative humidity. First, the real impedance or resistance from the x-intercept of the regression of the Nyquist plot was calculated. The proton conductivity (σ) (S/cm) was calculated using eq. (5), where L (cm) is the membrane thickness, A (cm^2) the membrane area, and R (Ω) the real impedance or resistance.

$$\sigma = \frac{L}{(AR)} \quad (5)$$

Analytical Ionic Concentration. The analytical ionic concentration of the wet membranes was calculated using eq. (6).

$$[\text{ionic domain}] = \frac{W_{dry}\ (g)}{V_{wet}(cm^3)} \times \text{IEC}\left(\frac{\text{mmol}}{\text{g}}\right) \quad (6)$$

where W_{dry} is the weight of the dry membrane and V_{wet} is the volume of the wet membrane.

Effective Proton Mobility. The effective proton mobility of the wet membranes (μ_{eff}) was calculated using eq. (7).

$$\mu_{eff}\left(\frac{cm^2}{s\,V}\right) = \frac{\sigma\ (S/cm)}{F[\text{ionic domain}]} \quad (7)$$

where F is Faraday's constant and σ (S/cm) is the proton conductivity.

Methanol Permeability. The methanol permeability was measured using a side-by-side diffusion cell.[18] Before the experiments, the membranes were hydrated in DI water and then placed between the sides of the diffusion cell. One side of the cell contained a 2.0 M methanol solution and the other side DI water. The concentration of methanol in the DI water-side was time-monitored using a gas chromatograph (GC) equipped with a thermal conductivity detector (Shimadzu GC-8). Permeability values were determined from the slope of the concentration of methanol in the receptor cell with time [$C_B(t)$] [eq. (8)]. C_A is the concentration of methanol in the donor compartment, L (cm) the membrane thickness, V_B (cm^3) the volume of the receptor compartment, A (cm^2) the cross-sectional area of the membrane, D (cm^2/s) the methanol diffusion coefficient, and P (cm^2/s) the methanol permeability.

$$\frac{C_B(t)V_BL}{C_AA} = P\left(t - \frac{L^2}{6D}\right) \quad (8)$$

RESULTS AND DISCUSSION

Elemental Analysis

The sulfonation percentages were calculated from the EA results of C, H, O, and S. The mole % sulfonation was 100% for all the membranes reported in this study. Hundred percent of sulfonation corresponds to one sulfonic group substitution for each aromatic unit.

Fourier Transform Infrared

FT-IR spectroscopy was used to identify the nature of the different chemical groups in the polymer, especially the presence of the sulfonic group on sulfonation. Table II shows the characteristic vibration bands of the unsulfonated and sulfonated membranes. The presence of the sulfonic group was confirmed for SA by the presence of four characteristic bands at: 1226.7, 1120.6, 1025.8, and 100.3 cm^{-1}.[20,24] The bands at 1226.7 and 1120.6 cm^{-1} correspond to the symmetric stretching vibrations of the O═S═O, and the bands at 1025.8 and 100.3 cm^{-1} correspond to the asymmetric stretching vibrations of the O═S═O. A characteristic band at 832.1 cm^{-1} shows that the sulfonic group is in the para position of the aromatic group. Table II also shows that on sulfonation, the band at 1726 cm^{-1} (which corresponds to the ketone of the ester group) shifted to a lower

Table II. FTIR Vibrations Bands (cm^{-1})

Sample	O=S=O symmetric	O=S=O symmetric	O=S=O asymmetric	O=S=O asymmetric	—O—	—O—	C=O
A	—	—	—	—	1084.0	1146.0	1726.0
SA	1226.7	1120.6	1025.8	1000.3	1084.0	1150.0	1721.0
BAB 18	—	—	—	—	1140.0	1171.0	1726.0
SBAB 18	1204.0	1120.6	1024.5	1000.3	1051.0	1181.0	1718.0
BAB 31	—	—	—	—	1152.0	1171.0	1726.0
SBAB 31	1210.0	1120.6	1024.5	1000.3	1158.0	1176.0	1718.0

wavenumber (1721 cm^{-1}) and the band at 1146 cm^{-1} shifted to a higher wavenumber (1150 cm^{-1}) (which corresponds to the ether group).[20,24] This implies that both the ester and the ether groups are interacting with the sulfonic group.

Table II also shows the vibrations for BAB 18, BAB 31, SBAB 18, and SBAB 31. Table II also shows that in the spectrum of the block copolymers BAB 18 and BAB 31, the characteristic band for the ether and the ester shifted indicating that PS affects the resulting polymer rearrangement. The FT-IR spectra of the block copolymers show that once the block polymers are sulfonated these characteristic bands shifted, suggesting a different rearrangement in the polymer matrix. The FT-IR results confirmed that all the block copolymers studied are interconnected in different ways.

Ion Exchange Capacity

IEC was measured for the unsulfonated and sulfonated membranes and the results are presented in Figure 3. The IEC of the membranes were listed in Table III. As expected, the IEC decreased with an increase of PS (B) [Figure 3(A)], as there are less overall ionic domains. On sulfonation of B, the IEC increased with an increase of B (increase of sulfonic domains). The highest IEC was 3.1 mequiv g^{-1} for SBAB 31, which was significantly higher than Nafion® 117 (0.92 mequiv g^{-1}).[3] The IEC results indicate that the sulfonated membranes possess more available sites for the transport of H^+, due to the additional sulfonic groups in the membrane [Figure 3(C)].

Water Uptake and Water Content

Water uptake is an important property for a PEM because water facilitates the transport of protons through the membrane.[20] However, excessive water uptake of the membranes can reduce the proton conductivity.[12] Figure 3 and Table III showed the water uptake of the unsulfonated and sulfonated membranes. As expected, the water uptake of the unsulfonated membranes decreases as B percentage increases [Figure 3(B)]. The water uptake of sulfonated A (SA) was not considered because the polymer was soluble in water after 18 h. Furthermore, the water absorption of the sulfonated membranes increased with increase of B percentage. SBAB 31 had the highest water uptake about 170% which was higher than Nafion® 117.[3] In addition, the water uptake of the membranes increased with increasing IEC [Figure 4(A)]. On incorporating PS (B), the water uptake was

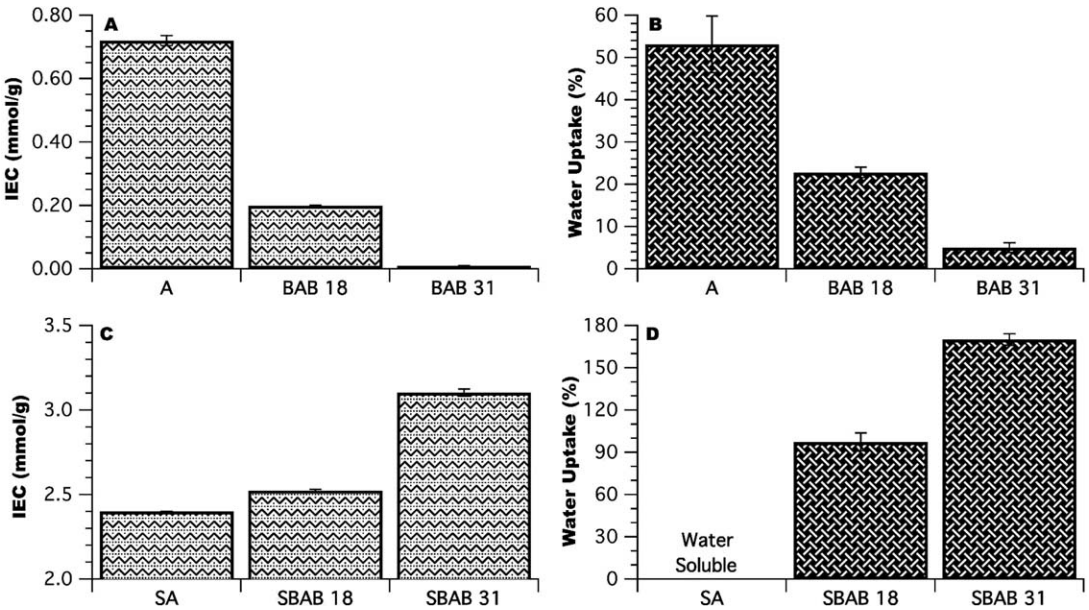

Figure 3. (A) IEC (mmol/g) of unsulfonated membranes, (B) Water Uptake (%) of unsulfonated membranes, (C) IEC (mmol/g) of sulfonated membranes, and (D) Water Uptake (%) of sulfonated membranes.

Table III. IEC and Water Absorption Values for the Membranes

Membrane	IEC (mmol/g)	Water uptake (wt %)	λ ([H_2O]/[ionic group])
A	0.72 ± 0.016	53.14 ± 6.69	41.00
BAB 18	0.20 ± 0.001	22.81± 1.25	63.36
BAB 31	0.01 ± 0.001	5.02 ±1.15	278.89
SA	2.4 ± 0.001	—	—
SBAB 18	2.5 ± 0.007	97.44 ± 6.38	21.45
SBAB 31	3.1 ± 0.021	170.07 ± 4.07	30.44

reduced, due to the molecular structure of the styrene. Conversely, incorporating sulfonic groups to styrene resulted in extensive hydrogen bond domains causing the increase in water content and IEC.

To analyze the effect of water in the membranes, water content was calculated. The water content represents the moles of water per ionic domain. These results show an exponential decay in the amount of water per ionic group versus IEC [Figure 4(B)]. As the number of ionic domains increases, the moles of water per ionic domain reach a stable value. Other investigators have found the importance of water in the transport of protons through the membrane.[25] Peckham suggested a λ value around 10–20, for enhanced water effect on the proton conductivity.[8] The effect of water content on the proton conductivity of the studied membranes will be further discussed ahead.

Morphology Characterization

Morphology influences the transport properties of a DMFC due to the changes in the distances of the ionic domains and their distribution. The aggregation of ionic domains has been extensive studied by SAXS and AFM.[26] SAXS experiments were performed to the dry and fully hydrated membranes. As observed in Figure 5, the unsulfonated membranes possess three interstitial distances. Table IV summarizes the scattering vectors and the Bragg's interstitial distances for the dry membranes. The first distance corresponds to the largest ionic domain and the slope after this peak is used to understand the morphology of the membranes. The second distance obtained with SAXS corresponds to the aggregation of smaller ionic domains and the third distance has been described by other investigators[27] to represent aromatic domains. The second and third distances do not significantly change for all the unsulfonated membranes, while the first distance decreases on increasing the amount of PS (BAB 31) as the additional non-ionic domains produce additional phase segregation that decreases the size of the largest ionic domains. Figure 5 also shows that the slope of the graph after the first peak is very similar for the unsulfonated membranes, but changes once the polymer is sulfonated, suggesting that the morphology of the polymer changes on sulfonation. This slope indicates that the block copolymer is comprised of hydrophobic and hydrophilic domains that exhibit phase separation because of the incompatible domains. Additionally, SAXS results confirmed that although there are unique interstitial distances due to the ionic interconnections in the membrane, the overall polymer morphology is amorphous. Luu[28] reported that the phase separation facilitates the formation of continuous ion channels that allow the transport of protons through the membrane and further improve their performance in fuel cells. As seen in Figure 5, once the block copolymer (SBAB 18 and SBAB 31) is sulfonated, a new distance appears. The measurement of this new distance is between 4.22 and 4.27 nm. This new distance suggests that once the PS is sulfonated the polymer has the capacity to interconnect with the ether and ester groups of the first block. These results agree with the previously discussed FT-IR results that confirmed new interconnections with the ether and ester groups on sulfonation.

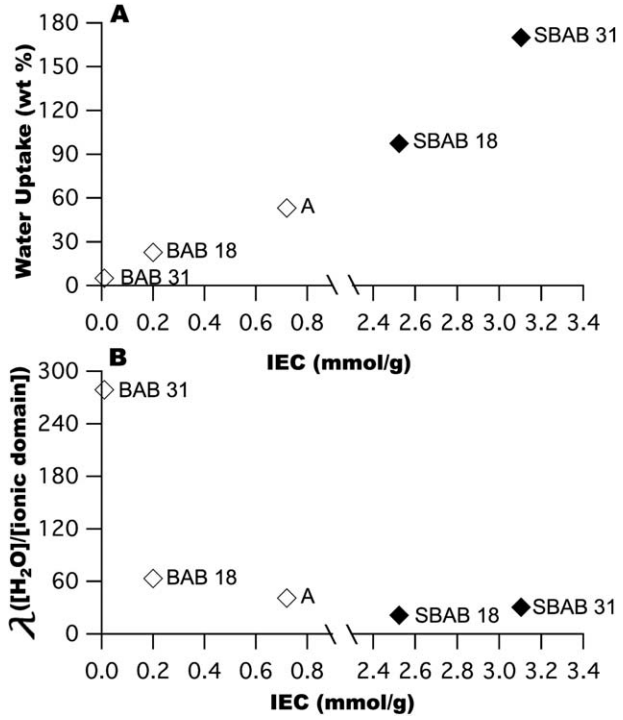

Figure 4. (A) Water Uptake (wt %) versus IEC (mmol/g), (B) λ ([H_2O]/[ionic group]) versus IEC (mmol/g).

Figure 5 also shows the SAXS results for the fully hydrated membranes while Table V summarizes the distances for the fully hydrated membranes. As expected, on hydration the morphology of the membranes changes. In some cases, the changes in morphology on hydration is significant, such as in BAB 31 and SBAB 18 (recall that SA is water-soluble). The ionic interconnections are significantly influenced by the presence of water but Guiner or Porod models do not show significant differences

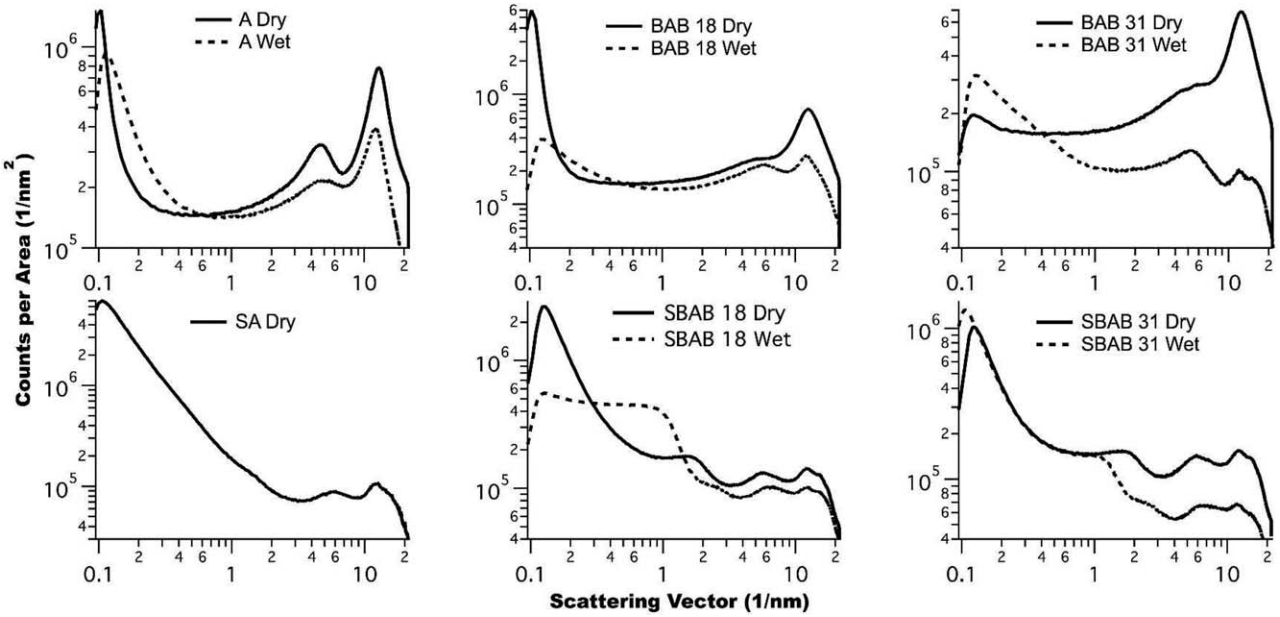

Figure 5. SAXS profiles for the dry and wet membranes.

in the resulting values on hydration due to the overall amorphous nature of the polymer.

The phase images for the unsulfonated and sulfonated membranes were obtained using AFM in AC mode (Figure 6). The variation in the phase images between A, BAB 18, and BAB 31 might be related to the changes in morphology upon the addition of PS. BAB 18 and BAB 31 show similar phase images because the only change is the percentage of PS. Once the polymer is sulfonated, there are significant differences in comparison with the unsulfonated polymers. SAXS results show that the SBAB 18 and SBAB 31 present a new distance that may be related to the interconnection of the sulfonic groups with the ether and the ester groups. These interconnections are observed in the phase images of Figure 6.

Transport Properties

Proton conductivity and methanol permeability were measured to evaluate the transport properties for DMFC applications. Low methanol permeability and high proton conductivity are desired for proper operation of a DMFC.[8] As shown in Figure 7(A) and Table VI, the proton conductivity for the unsulfonated membranes decreased with an increase of B, as the overall ionic domains and IEC decrease. Upon sulfonation the proton conductivity increased until 0.077 and then decreased [Figure 7(D)]. In fact, proton conductivity shows the same behavior with the IEC, water uptake and ionic domain concentration [Figure 7(B,C,F)]. The proton conductivity shows an inversely proportional relationship with water content per ionic domain [Figure 7(E)]. Other investigators have observed that although water is critical for the transport of protons through the membrane, only the water bound to the ionic domains helps in the transport of protons through the PEM.[23,27–29] Also, other investigators have also observed a maxima in the proton conductivity versus sulfonation level and have also explained it with complex or non-oriented morphology that disturbs the path for protons to be conducted.[24,30] This behavior will be further explained studying the proton mobility ahead in this article. The highest proton conductivity was 0.077 S/cm for SBAB 18, which was higher than Nafion® 117 (0.05 S/cm), but all the sulfonated membranes studied produced higher proton conductivity than Nafion® 117. It should also be pointed out that all the membranes studied produced

Table IV. Scattering Vectors (1/nm) and Bragg Distances (nm) for the Dry Membranes

Sample	Q_1 (1/nm)	D_1 (nm)	Q_2 (1/nm)	D_2 (nm)	Q_3 (1/nm)	D_3 (nm)	Q_4 (1/nm)	D_4 (nm)
A	0.0973	64.53	4.54	1.38	13.10	0.48	—	—
BAB 18	0.103	61.00	4.38	1.43	12.7	0.49	—	—
BAB 31	0.124	50.67	4.74	1.33	12.5	0.50	—	—
SA	0.119	52.80	4.50	1.40	13.0	0.48	—	—
SBAB 18	0.129	48.71	1.47	4.27	5.11	1.23	10.9	0.58
SBAB 31	0.121	51.93	1.49	4.22	5.85	1.07	11.9	0.53

Table V. Scattering Vectors (1/nm) and Bragg Distances (nm) for the Fully Hydrated Membranes

Sample	Q_1 (1/nm)	D_1 (nm)	Q_2 (1/nm)	D_2 (nm)	Q_3 (1/nm)	D_3 (nm)	Q_4 (1/nm)	D_4 (nm)	Q_5 (1/nm)	D_5 (nm)
A	0.111	56.61	4.53	1.39	13.10	0.48	—	—	—	—
BAB 18	0.128	49.09	4.15	1.51	12.4	0.51	—	—	—	—
BAB 31	0.125	50.27	5.10	1.23	12.4	0.51	—	—	—	—
SA	—	—	—	—	—	—	—	—	—	—
SBAB 18	0.126	49.87	1.00	6.28	2.60	2.42	5.37	1.17	11.1	0.57
SBAB 31	0.105	59.84	0.917	6.85	2.97	2.12	6.23	1.01	12.1	0.52

proton conductivities higher than 10^{-2} S/cm, which is the lowest acceptable value for fuel cell usage.[31]

Before we discuss the effect of hydration level on the proton conductivity, it might be important to evaluate the effective proton mobility (μ_{eff}). The effective proton mobility provides useful information about the ionic domain dissociation, ionic channel tortuosity and spatial proximity of neighboring ionic sites.[27] Figure 8(A) shows the relation between μ_{eff} and IEC. The effective proton mobility can be affected by the tethering of the ionic domains, the effective mean-path,[32] and the distance between ionic domains.[8] SBAB 31 has the largest amount of available ionic sites for interconnection in the polymer but the lowest μ_{eff}. Figure 8(B) suggests that as the concentration of ionic domains increases, the degree of tortuosity of the proton conduction pathways increases, decreasing the effective proton mobility. Figure 8(C) shows that SBAB 18 has the highest value of proton conductivity and the lowest value of effective proton mobility, which suggests that there is an optimum value of interconnections for the transport of protons through the membrane with the help of water.

The proton conductivity was further studied at different hydration levels (therefore, different λ's), to understand the causes for the differences between the proton conductivity of SBAB 18 and SBAB 31. Figure 9(A) shows that the proton mobility increases with an increase in λ. Peckham observed the same behavior and suggested that increasing λ leads to an increase in the proton mobility, but also a dilution of available acidic sites.[30] Figure 9(B) shows that the proton conductivity has an optimum value with λ around 20 for both SBAB 18 and SBAB31. Peckham *et al.* observed that in the region of 10-20, water has a beneficial effect in the proton conductivity.[8] Figure 9(C) shows the relation between proton conductivity and proton mobility and we can see that there is also an optimum value for proton mobility. When the dilution of the ionic domains becomes too high, the proton conductivity begins to decrease.

Figure 10(A) shows the methanol permeability for the unsulfonated membranes and the values are also summarized in Table VI. The results show that the addition of PS to A decreases the methanol permeability. Upon sulfonation, the methanol

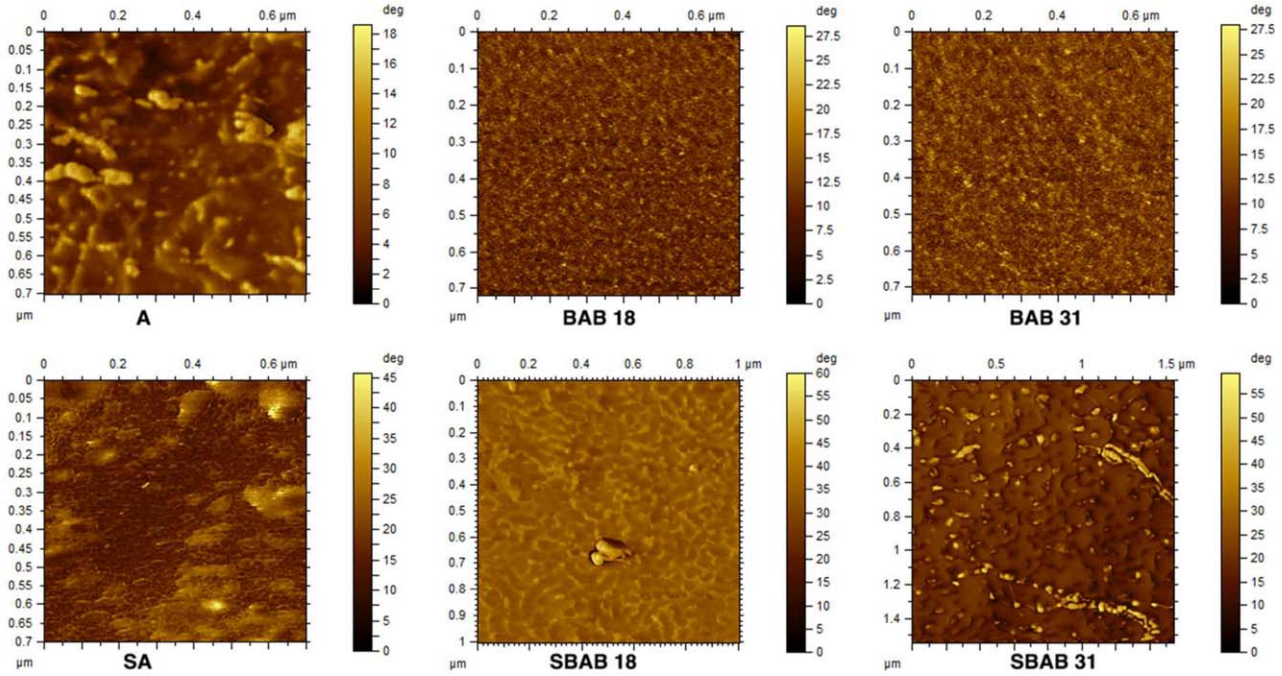

Figure 6. AFM profiles for unsulfonated and sulfonated membranes. [Color figure can be viewed at wileyonlinelibrary.com.]

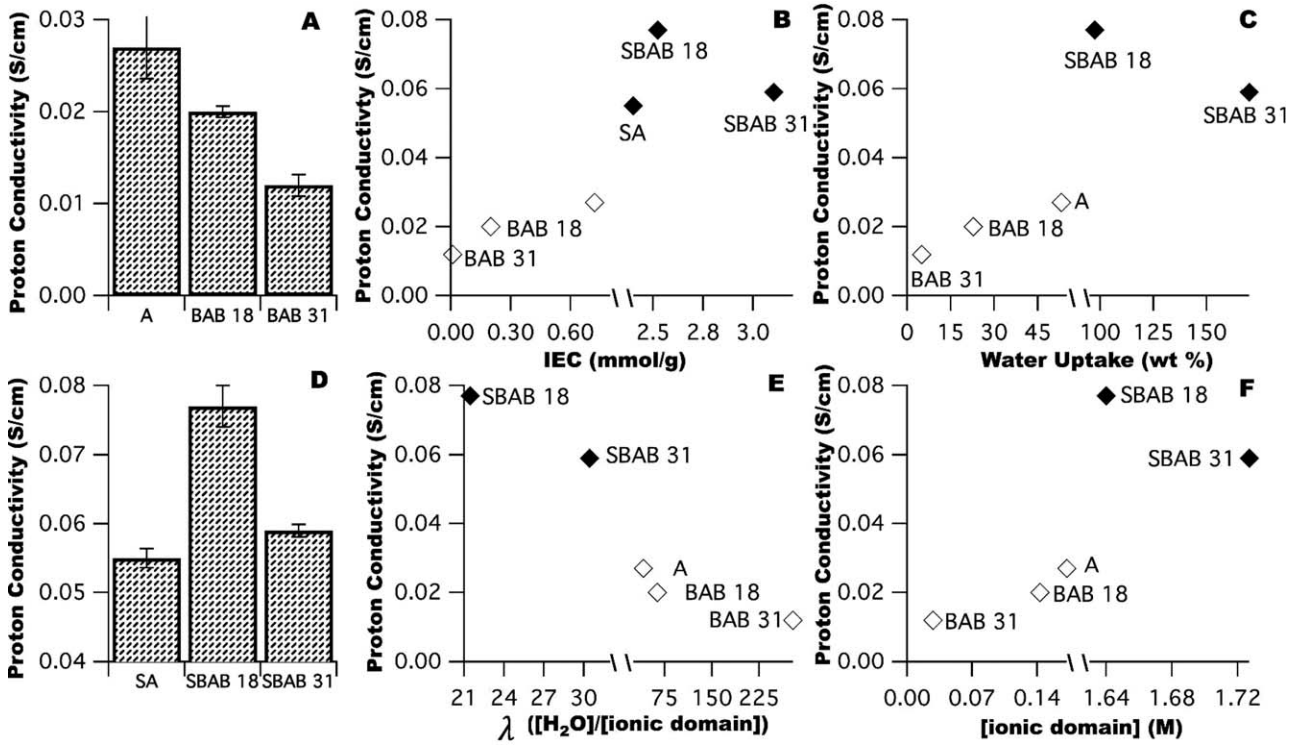

Figure 7. (A) Proton Conductivity (S/cm) of unsulfonated membranes, (B) Proton Conductivity (S/cm) versus IEC (mmol/g), (C) Proton Conductivity (S/cm) versus Water Uptake (wt %), (D) Proton Conductivity (S/cm) of sulfonated membranes, (E) Proton Conductivity (S/cm) versus λ ([H_2O]/[ionic group]), and (F) Proton Conductivity (S/cm) versus [ionic group] [M].

permeability increases [Figure 10(D)] and the evaluation with IEC, water uptake and overall available ionic sites also increases [Figure 10(B,C,F)]. There appears to be a certain threshold value of ions, IEC and water uptake for the methanol permeability to significantly increase. The largest methanol permeability occurred with SA, which was soluble in water. The SA membrane was also soluble in methanol after 6 h. The methanol permeability experiments were conducted for 2 h and during that time the integrity of the membranes remained intact after completing the measurements. The other sulfonated membranes (SBAB 18 and SBAB 31) remained insoluble in methanol for at least 24 h. Figure 10(E) shows that the methanol permeability is not as sensitive to λ as the proton conductivity. Proton transport critically depends on the amount of water per ionic group, but the methanol permeability is more sensitive to free volume, which is influenced by the concentration of ionic sites and the overall amount of water in the membrane.[20] As previously stated in Figure 5 and Table IV, there were four interstitial distances in the sulfonated membranes (SBAB 18 and SBAB 31). D_2 and D_3 distances are related to the tortuosity of the membrane and could be related to the free volume of the membrane, suggesting that the re-arrangement inside the membrane for SBAB 18 and SBAB 31 is different (Table IV). This was also supported with the AFM phase images (Figure 6). The lower methanol permeability was 3.94×10^{-8} cm^2/s for BAB 31, which was lower than Nafion® 117 (1.98×10^{-6} cm^2/s).

The selectivity (ratio of proton conductivity over methanol permeability) of the membranes was calculated to evaluate the transport performance of the membranes. The resulting values were normalized with the corresponding value of the state-of-the-art PEM Nafion®. The normalized selectivities were compared to evaluate the performance of the membranes and the corresponding changes with the variables studied (Table VI and Figure 11). Figure 11(A) shows the normalized selectivity for the unsulfonated membranes. BAB 18 shows the highest value

Table VI. Transport Properties

Membrane	Proton conductivity (S/cm)	Effective proton mobility μ_{eff}	Methanol permeability (cm^2/s)	Normalized selectivity
A	0.027 ± 0.0034	1.63×10^{-3}	$8.70 \times 10^{-7} \pm 4 \times 10^{-8}$	0.92
BAB 18	0.020 ± 0.0006	1.48×10^{-3}	$8.28 \times 10^{-8} \pm 7 \times 10^{-9}$	15.30
BAB 31	0.012 ± 0.0012	4.60×10^{-3}	$3.94 \times 10^{-8} \pm 2 \times 10^{-8}$	4.38
SA	0.055 ± 0.0014	—	$1.67 \times 10^{-6} \pm 2 \times 10^{-7}$	0.97
SBAB 18	0.077 ± 0.0030	3.52×10^{-4}	$5.36 \times 10^{-7} \pm 3 \times 10^{-8}$	4.25
SBAB 31	0.059 ± 0.0009	4.87×10^{-4}	$1.50 \times 10^{-6} \pm 1 \times 10^{-7}$	1.16

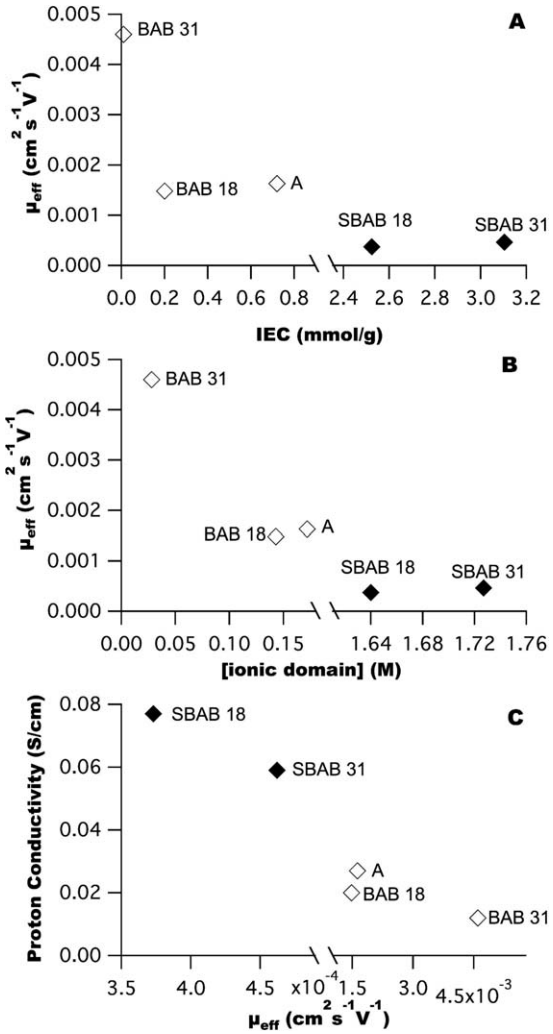

Figure 8. (A) μ_{eff} versus IEC (mmol/g), (B) μ_{eff} versus [ionic group] [M] and (C) Proton Conductivity versus μ_{eff}.

of normalized selectivity, 15.3 times better than the state-of-the-art Nafion®, due to its high proton conductivity and low methanol permeability. Figure 11(B) shows that the relationship between proton conductivity and methanol permeability for BAB 18 and BAB 31 is proportional, suggesting similar transport mechanisms for protons and methanol for these two membranes. The comparison with A shows a larger increase in methanol permeability than in proton conductivity. On sulfonation, there was also an optimal normalized selectivity membrane [Figure 11(C)]. SBAB 18 showed the highest value of normalized selectivity (4.25) for the sulfonated membranes. Figure 11(D) shows an inverse relationship between the proton conductivity and the methanol permeability for the sulfonated membranes studied, suggesting different and unique transport mechanisms for these multi-ionic polymer membranes with unique morphology and water content.

CONCLUSIONS

This research studied the morphology, water content and transport properties of PS-*b*-PEGPEM-*b*-PS membranes as a function of block composition and sulfonation level. An increase in the amount of PS decreases the IEC, water absorption, proton conductivity, and methanol permeability due to a reduction in the ionic interconnections in the unsulfonated membranes. Once the polymers were sulfonated, the transport mechanism of methanol and protons were significantly altered due to the morphological differences and water content produced by the complex multi-ionic domain nanostructure. The proton conductivity remained sensitive to the amount of water per ionic domain (optimum λ close to 20), regardless of the nature of the ion (e.g., ethers, esters, or sulfonic groups). The methanol permeability showed sensitivity to the overall number of ions and water, which influenced the morphology of the membrane. The combination of chemistry (multi-ionic

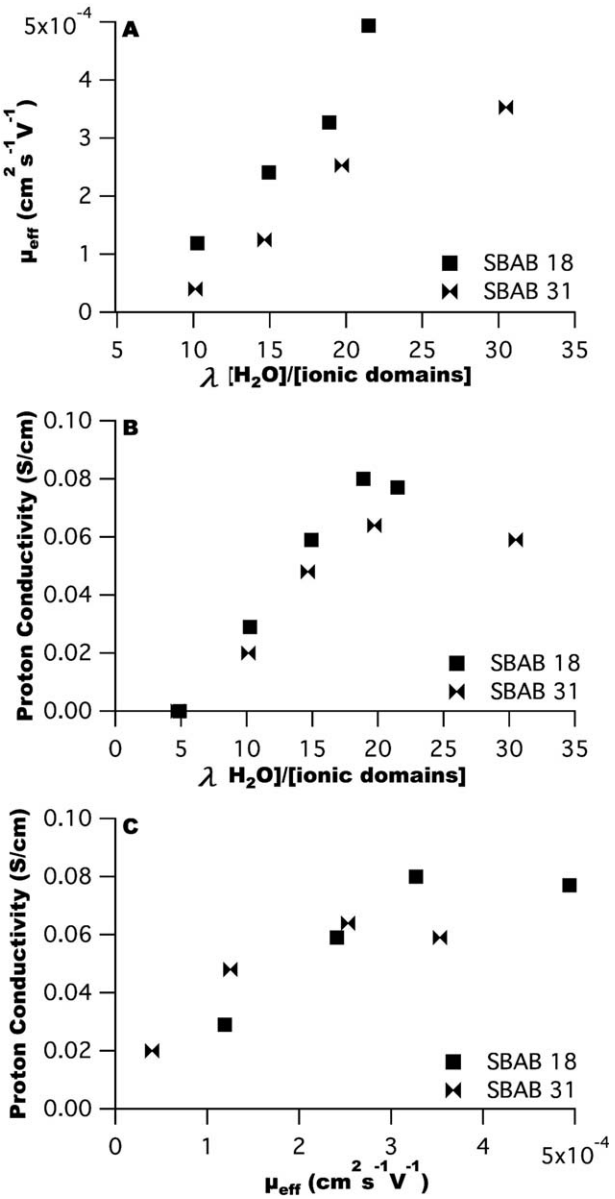

Figure 9. (A) μ_{eff} (cm^2 s^{-1} V^{-1}) versus λ([H_2O]/[ionic domain]), (B) Proton conductivity (S/cm) versus λ ([H_2O]/[ionic domain]) and (C) Proton conductivity (S/cm) versus μ_{eff} (cm^2 s^{-1} V^{-1}).

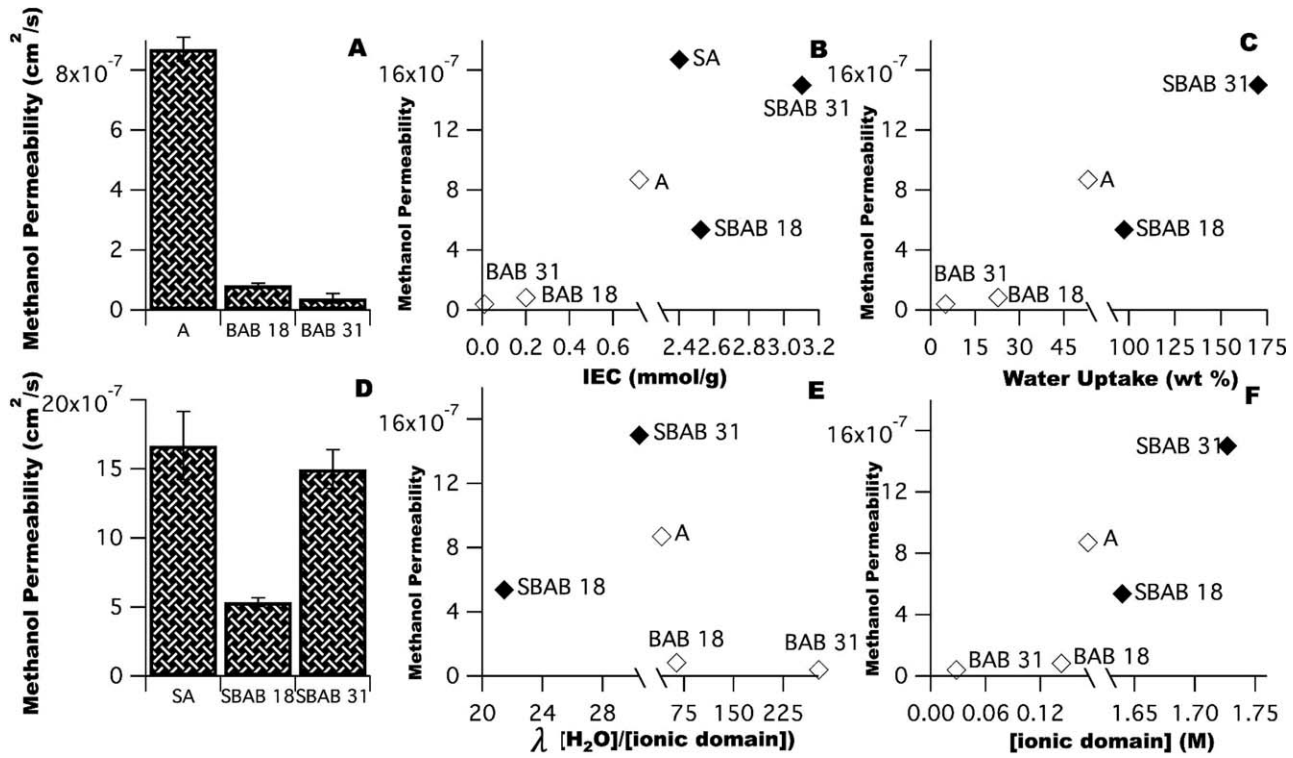

Figure 10. (A) Methanol Permeability (cm^2/s) for unsulfonated membranes, (B) Methanol Permeability (cm^2/s) versus IEC (mmol/g), (C) Methanol Permeability (cm^2/s) versus Water Uptake (wt %), (D) Methanol Permeability (cm^2/s) for sulfonated membranes, (E) Methanol Permeability (cm^2/s) versus λ ($[H_2O]/[$ionic group$]$), and (F) Methanol Permeability (cm^2/s) versus [ionic group] [M].

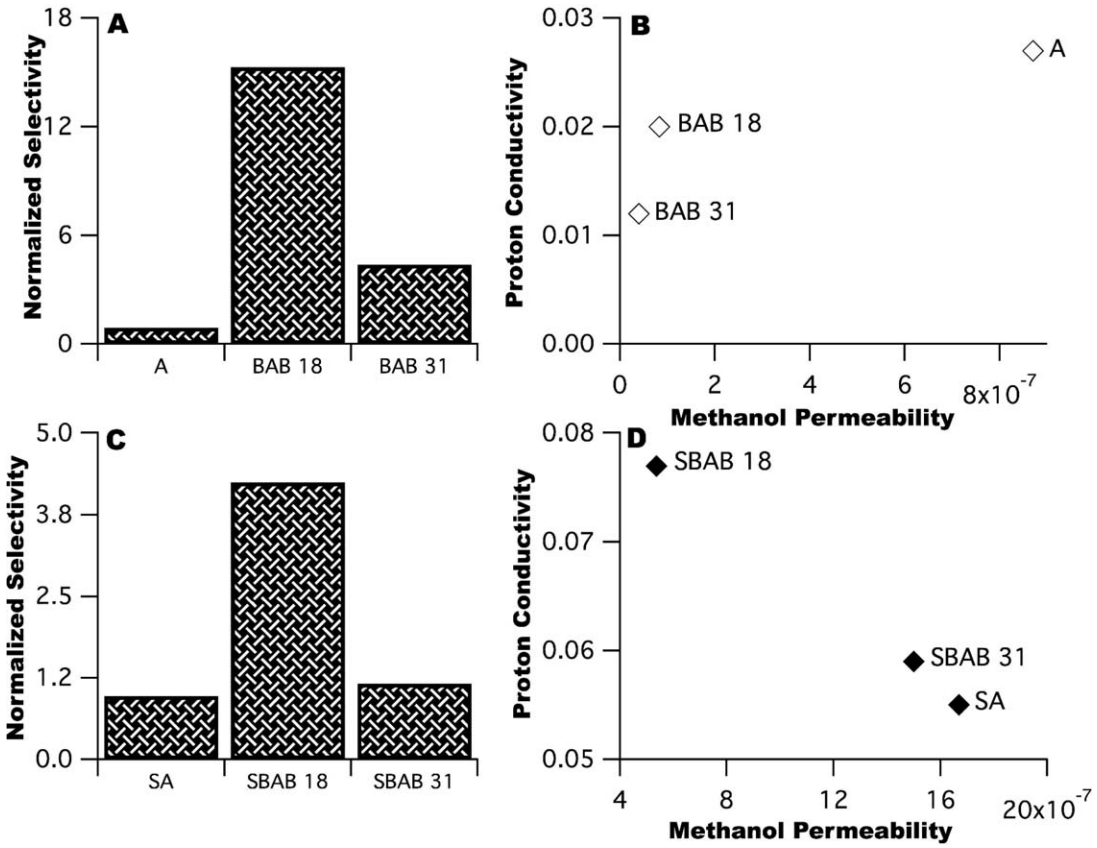

Figure 11. (A) Normalized selectivity for unsulfonated membranes, (B) Proton Conductivity (S/cm) versus Methanol Permeability (cm^2/s), (C) Normalized selectivity of sulfonated membranes, and (D) Proton Conductivity (S/cm) of sulfonated membranes.

domains), water content, and morphology allowed for transport property selectivities (proton conductivity over methanol permeability) for PS-*b*-PEGPEM-*b*-PS 18% to be 15 times better than the state-of-the-art Nafion®.

ACKNOWLEDGMENTS

This material is based on work supported by the U.S. Army Research Laboratory and the U.S. Army Research Office under contract/Grant numbers W911-NF-13-10166 and W911-NF-14-10076.

REFERENCES

1. Zhang, H.; Ma, C.; Wang, J.; Wang, X.; Bai, H.; Liu, J. *Int. J. Hydrogen Energy* **2014**, *39*, 974.
2. Jothi, P. R.; Dharmalingam, S. *J. Membr. Sci.* **2014**, *450*, 389.
3. Li, H.; Cui, Z.; Zhao, C.; Wu, J.; Fu, T.; Zhang, Y.; Shao, K.; Zhang, H.; Na, H.; Xing, W. *J. Membr. Sci.* **2009**, *343*, 164.
4. Ismail, A. F.; Anam, M. N.; Norddin, M.; Juhana, J.; Matsuura, T. In Membrane Modification; CRC Press, **2012**; Vol. 409.
5. Basile, A.; Iulianelli, A. In Fuel Cell Research Trends; Vasquez, L. O., Ed.; Nova Science Publishers, Inc., New York, **2007**; pp. 135–160.
6. Ismail, A. F.; Othman, N. H.; Mustafa, A. *J. Membr. Sci.* **2009**, *329*, 18.
7. Haldorai, Y.; Shim, J. J.; Lim, K. T. *J. Supercrit. Fluids* **2012**, *71*, 45.
8. Peckham, T. J.; Yang, Y.; Holdcroft, S. In Proton Exchange Membrane Fuel Cells Materials Properties and Performance; CRC Press, **2010**; pp 305–342.
9. Peighambardoust, S. J.; Rowshanzamir, S.; Amjadi, M. *Int. J. Hydrogen Energy* **2010**, *35*, 9349.
10. Xing, P.; Robertson, G. P.; Guiver, M. D.; Mikhailenko, S. D.; Wang, K.; Kaliaguine, S. *J. Membr. Sci.* **2004**, *229*, 95.
11. Knauth, P.; Sgreccia, E.; Donnadio, A.; Casciola, M.; Di Vona, M. L. *J. Electrochem. Soc.* **2011**, *158*, B159.
12. Peckham, T. J.; Schmeisser, J.; Holdcroft, S. *J. Phys. Chem. B* **2008**, *112*, 2848.
13. Bose, A. B.; Gopu, S.; Li, W. *J. Power Sources* **2014**, *263*, 217.
14. Guerrero-Gutiérrez, E. M. A.; Pérez-Pérez, M.; Suleiman, D. *J. Appl. Polym. Sci.* **2015**, *132*, DOI: 10.1002/app.42046.
15. Zhao, C.; Lin, H.; Shao, K.; Li, X.; Ni, H.; Wang, Z.; Na, H. *J. Power Sources* **2006**, *162*, 1003.
16. Du, L.; Yan, X.; He, G.; Wu, X.; Hu, Z.; Wang, Y. *Int. J. Hydrogen Energy* **2012**, *37*, 11853.
17. Kreuer, K. D. *J. Membr. Sci.* **2001**, *185*, 29.
18. Wu, H. L.; Ma, C. C. M.; Li, C. H.; Lee, T. M.; Chen, C. Y.; Chiang, C. L.; Wu, C. *J. Membr. Sci.* **2006**, *280*, 501.
19. Yee, R. S. L.; Zhang, K.; Ladewig, B. P. *Membranes* **2013**, *3*, 182.
20. Pérez-Pérez, M.; Suleiman, D. *J. Membr. Sci.* **2015**, *493*, 414.
21. Gupta, B.; Gautam, D.; Ikram, S. *Indian J. Chem. Technol.* **2014**, *21*, 176.
22. Elabd, Y. A.; Napadensky, E.; Walker, C. W.; Winey, K. I. *Macromolecules* **2006**, *39*, 399.
23. Elabd, Y. A.; Napadensky, E. *Polymer* **2004**, *45*, 3037.
24. Avilés-Barreto, S. L.; Suleiman, D. *J. Appl. Polym. Sci.* **2013**, *129*, 2294.
25. Tripathi, B. P.; Kumar, M.; Shahi, V. K. *J. Membr. Sci.* **2009**, *327*, 145.
26. Eisenberg, A. *Macromolecules* **1970**, *3*, 147.
27. Tsang, E. M. W.; Zhang, Z.; Yang, A. C. C.; Shi, Z.; Peckham, T. J.; Narimani, R.; Frisken, B. J.; Holdcroft, S. *Macromolecules* **2009**, *42*, 9467.
28. Luu, D. X.; Cho, E. B.; Han, O. H.; Kim, D. *J. Phys. Chem. B* **2009**, *113*, 10072.
29. Avilés-Barreto, S. L.; Suleiman, D. *J. Membr. Sci.* **2015**, *474*, 92.
30. Peckham, T. J.; Schmeisser, J.; Holdcroft, S. *J. Mater. Chem.* **2007**, *17*, 3255.
31. Zhang, H.; Li, X.; Zhao, C.; Fu, T.; Shi, Y.; Na, H. *J. Membr. Sci.* **2008**, *308*, 66.
32. Knauth, P. D.; Vona, M. L. *ECS Trans.* **2013**, *50*, 1037.